Journal of the Mechanics and Physics of Solids 138 (2020) 103899

Contents lists available at ScienceDirect

Journal of the Mechanics and Physics of Solids

journal homepage: www.elsevier.com/locate/jmps

Lattice strains and diffraction elastic constants of cubic polycrystals

Yin Zhang[a], Wen Chen[b], David L. McDowell[a], Y. Morris Wang[c], Ting Zhu[a,*]

[a] Woodruff School of Mechanical Engineering, Georgia Institute of Technology, Atlanta, GA 30332, USA
[b] Department of Mechanical and Industrial Engineering, University of Massachusetts, Amherst, MA 01003, USA
[c] Lawrence Livermore National Laboratory, Livermore, CA 94550, USA

ARTICLE INFO

Article history:
Received 22 November 2019
Revised 19 January 2020
Accepted 6 February 2020
Available online 11 February 2020

ABSTRACT

In situ synchrotron X-ray and neutron diffraction experiments provide a powerful approach to measure lattice strains in bulk polycrystalline materials. They are being increasingly used for quantitative characterization of microscale deformation within and between grains and phases. Here we use a self-consistent micromechanics model to obtain a general analytic solution of the grain-level lattice strains and diffraction elastic constants for a broad class of elastically isotropic polycrystals with cubic crystal symmetry. This analytic solution reveals a direct linear relationship between the reciprocal of the elastic diffraction constant and the orientation index parameter along the direction of any diffraction vector, including tensile loading and transverse directions. The straightforward numerical implementation of this solution provides diffraction elastic constants for 26 representative cubic polycrystals. Analytic solutions of this kind can serve to benchmark *in situ* diffraction measurements of lattice strains and also facilitate high-throughput studies of microscale stresses and diffraction elastic constants in polycrystalline materials.

1. Introduction

In situ synchrotron X-ray diffraction (SXRD) and neutron diffraction experiments are widely used in a broad range of disciplines, including materials science, geophysics, environmental science, biophysics and others (Allen et al., 1985; Ice et al., 2011). They can provide direct measurements of lattice strains in bulk polycrystalline materials (Clausen et al., 1998; Dye et al., 2001; Hommer et al., 2019; Li et al., 2018). In the elastic regime, the lattice strains of individual grain families with specific orientation increase linearly with the macroscopically applied stress, as demonstrated, for example, by neutron diffraction of copper (Clausen et al., 1998), steel (Clausen et al., 1999; Daymond et al., 1997, 2000; Pang et al., 1998, 2000), nickel-based alloys (Holden et al., 1997, 1998), and SXRD of austenitic stainless steel (Chen et al., 2019; Wang et al., 2018b). These linear relationships are usually characterized by the so-called diffraction elastic constants (Behnken and Hauk, 1986; Bollenrath et al., 1967; DeWit, 1997; Gnaupel-Herold et al., 1998), which vary with the orientation of the grain family. The lattice strains and diffraction elastic constants have many possible uses in analysis of microscale residual stresses (Hu et al., 2016; Li et al., 2018) and progressive yielding (Chen et al., 2019; Wang et al., 2018b). They also provide a means of reversely determining the single crystal elastic constants of new materials (Wu et al., 2014) or materials with lower symmetries (Stebner et al., 2013). However, it is hard to find solutions for lattice strains and diffraction elastic constants of many

* Corresponding author.
E-mail address: ting.zhu@me.gatech.edu (T. Zhu).

https://doi.org/10.1016/j.jmps.2020.103899
0022-5096/

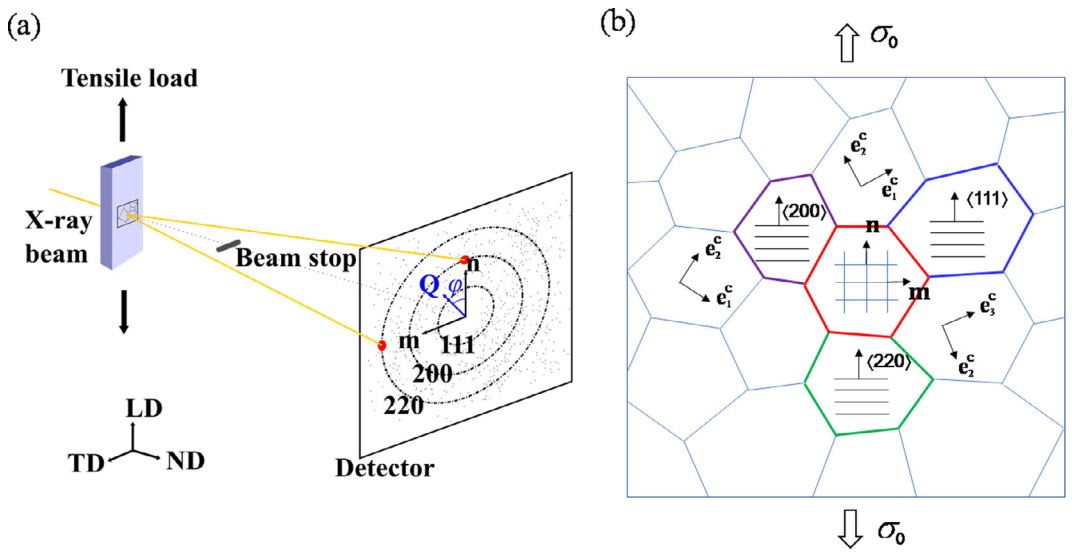

Fig. 1. Schematic diagrams of *in situ* SXRD measurements of lattice strains in a polycrystalline material. (a) Schematic of SXRD setup (Chen et al., 2019), showing an incident X-ray beam into a polycrystalline specimen diffracted to generate a series of Debye-Scherrer rings. The loading direction (denoted as LD), transverse direction (TD), and normal direction (ND) of the specimen are marked. In the detector plane, the unit normal vector **n** is along LD, **m** along TD, and a general diffraction vector **Q** deviates **n** by an angle φ. Note that the red diffraction spot at the top-center of the detector plane is actually produced by diffraction of lattice planes with poles slightly misaligned from the LD by a very small angle (less than 1° in typical SXRD measurements); a similar approximation is applied to other diffraction spots in the detector plane as well. (b) Two-dimensional cross section of an RVE in the tensile specimen in (a), subjected to a uniaxial tensile stress σ_0. Each grain is associated with a set of local orthonormal crystal basis vectors $\{\mathbf{e}_1^c, \mathbf{e}_2^c, \mathbf{e}_3^c\}$, and the out-of-plane basis vector is not shown. Representative grains in respective {200}, {220} and {111} families oriented along LD are marked.

materials in the literature. The demand for these solutions is expected to grow in the coming years, as *in situ* diffraction experiments can be used for high-throughput and data-analytics studies of the mechanical behavior of polycrystalline materials with complex compositions and microstructures, such as high-entropy alloys (Wang et al., 2018a; Wu et al., 2014), additively manufactured alloys (Brown et al., 2017; Chen et al., 2019; Wang et al., 2018b), heterogeneous nanostructured metals and alloys (Ma and Zhu, 2017; Wang et al., 2010), and others.

In this paper, we make a combined use of the classical Eshelby inclusion solution (Eshelby, 1957) and the self-consistent method of microstructure homogenization (Qu and Cherkaoui, 2006) to obtain a general analytic solution of grain-level lattice strains and diffraction elastic constants. This solution is applicable to a broad class of elastically isotropic polycrystals with cubic crystal symmetry, including face-centered cubic (FCC), body-centered cubic (BCC) and diamond cubic (DC) crystals. Bollenrath et al. (1967) obtained an analytic solution of diffraction elastic constants of cubic polycrystals using Kröner's self-consistent method (Kröner, 1960). De Wit gave alternative solutions of diffraction elastic constants (DeWit, 1997). But they did not provide the general analytic solution of lattice strains, and their derivations of the diffraction elastic constant solutions were not completely presented. The diffraction elastic constants can also be calculated using different numerical methods. One is based on the self-consistent polycrystal model that requires a numerical average of lattice strains in grains within the same family (Clausen et al., 1998). Another is based on the finite element polycrystal model that relies on a full numerical calculation of lattice strains in a polycrystalline aggregate (Li and O'Dowd, 2011). Nonetheless, the analytic solutions are highly desired for clear understanding and robust parametric studies of the lattice strain effects. Here we adopt a modern micromechanics approach (Qu and Cherkaoui, 2006) to obtain a general analytic solution of lattice strains and diffraction elastic constants for cubic polycrystals. This solution can be readily understood and applied. It only requires an input of the three independent elastic constants of a cubic crystal. The associated numerical results are validated by literature data as well as polycrystal elasticity finite element simulations. Since the present solution requires only simple algebraic calculations, one can pursue straightforward numerical calculations to determine lattice strains and diffraction elastic constants for any cubic polycrystals using a MATLAB code.[1]

2. Lattice strains and diffraction elastic constants

Fig. 1a shows the schematic diagram of *in situ* SXRD measurement of lattice strains in a polycrystalline specimen under uniaxial tension. An incident X-ray beam into the specimen is diffracted to generate a series of Debye-Scherrer rings (Margulies et al., 2001). Each diffraction spot (e.g., red dot) on a ring corresponds to a family of grains with a common

[1] A MATLAB code is published online with this paper. The code is used to calculate the diffraction elastic constants of cubic polycrystals, based on the analytic solutions presented in this work.

crystallographic plane, such as a {111} plane, oriented along a specific spatial direction, e.g., the loading direction (denoted as LD and represented by the unit normal vector **n**), the transverse direction (denoted as TD and represented by the unit normal vector **m**), or the direction along any diffraction vector **Q**. By tracking the change of lattice spacings during tensile loading, one can obtain the average lattice strains in different grain families as a function of applied load, and then calculate the stresses in these grain families using single crystal elastic constants. Fig. 1b shows a two-dimensional cross section of a representative volume element (RVE) in the tensile specimen. In a typical grain (highlighted in red) in this RVE, the unit normal vector **n** of a set of lattice planes is oriented along LD, and the unit normal vector **m** of another set of lattice planes is oriented along TD. Each grain is associated with an orthonormal basis $\{\mathbf{e}_1^c, \mathbf{e}_2^c, \mathbf{e}_3^c\}$ of the cubic lattice. Also plotted are the representative grains in different {*hkl*} grain families oriented along LD. Different grain families usually exhibit different lattice strains and diffraction elastic constants, due to the elastic anisotropy of grain crystals.

Consider a {*hkl*} grain family consisting of *N* grains in an RVE of a polycrystal (Fig. 1b). These grains are numbered by 1, ... α, ... *N*. To determine the average lattice strains and diffraction elastic constants in this grain family, one needs to obtain a linear tensorial relation between the macroscopic stress $\overline{\sigma}_{ij}$ and the strain $\varepsilon_{ij}^{(\alpha)}$ in the grain α, i.e.,

$$\varepsilon_{ij}^{(\alpha)} = U_{ijkl}^{(\alpha)} \overline{\sigma}_{kl} \tag{1}$$

where $U_{ijkl}^{(\alpha)}$ is the constrained compliance tensor of the grain α embedded in the polycrystal. It should be noted that under a macroscopically applied load, the strain response of the grain α in a polycrystal is not merely determined by single crystal elastic constants, since elastically anisotropic grains interact with each other to adjust local strains for accommodating their deformation incompatibility. Hence, $U_{ijkl}^{(\alpha)}$ is different from the single crystal compliance tensor $M_{ijkl}^{(\alpha)}$ and will be derived in Section 3. Also note that throughout this paper, all the index components of vectors and tensors are resolved in the local orthonormal basis of the grain crystal, e.g., $\{\mathbf{e}_1^{c,(\alpha)}, \mathbf{e}_2^{c,(\alpha)}, \mathbf{e}_3^{c,(\alpha)}\}$ in the representative grain α; the Einstein summation convention is used for repeated indices, except for repeated α, β and γ.

Under an applied uniaxial tensile stress σ_0 (Fig. 1b), the macroscopic stress $\overline{\sigma}_{ij}$ acting on the polycrystalline RVE can be expressed as

$$\overline{\sigma}_{ij} = \sigma_0 n_i^{(\alpha)} n_j^{(\alpha)} \tag{2}$$

where $n_i^{(\alpha)}$ denotes the components of the unit vector along LD resolved in terms of the local cubic basis of the grain α. The lattice strain $\varepsilon_{\mathrm{LD}}^{(\alpha)}$ along LD can be similarly resolved in terms of the local cubic basis as

$$\varepsilon_{\mathrm{LD}}^{(\alpha)} = \varepsilon_{ij}^{(\alpha)} n_i^{(\alpha)} n_j^{(\alpha)} \tag{3}$$

Substitution of Eqs. (1) and (2) into Eq. (3) yields

$$\varepsilon_{\mathrm{LD}}^{(\alpha)} = \sigma_0 U_{ijkl}^{(\alpha)} n_i^{(\alpha)} n_j^{(\alpha)} n_k^{(\alpha)} n_l^{(\alpha)} \tag{4}$$

The average lattice strain $\overline{\varepsilon}_{\mathrm{LD}}$ in the {*hkl*} grain family along LD is, therefore, given by

$$\overline{\varepsilon}_{\mathrm{LD}} = \frac{1}{N} \sum_{\alpha=1}^{N} \varepsilon_{\mathrm{LD}}^{(\alpha)} \tag{5}$$

The diffraction elastic constant along LD is defined as

$$\frac{1}{E_{\mathrm{LD}}^{hkl}} = \frac{\overline{\varepsilon}_{\mathrm{LD}}}{\sigma_0} \tag{6}$$

Combining Eqs. (4-6), one can express E_{LD}^{hkl} as

$$\frac{1}{E_{\mathrm{LD}}^{hkl}} = \frac{1}{N} \sum_{\alpha=1}^{N} U_{ijkl}^{(\alpha)} n_i^{(\alpha)} n_j^{(\alpha)} n_k^{(\alpha)} n_l^{(\alpha)} \tag{7}$$

once $U_{ijkl}^{(\alpha)}$ is specified.

3. General solution for the constrained compliance tensor U

As shown in Section 2, the constrained compliance tensor $U_{ijkl}^{(\alpha)}$ is key to determining the lattice strains and diffraction elastic constants for a cubic polycrystal. In this Section, a general solution of this compliance tensor is obtained using the direct notation. We consider a polycrystalline RVE with a given distribution of grain orientations. The anisotropic elasticity tensor of the grain α is denoted as $\mathbf{L}^{(\alpha)}$. As discussed earlier, the lattice strain response of this grain is not merely determined by $\mathbf{L}^{(\alpha)}$, since elastically anisotropic grains interact with each other to adjust local strains. To account for such grain interactions, we consider a representative grain in an RVE as a spherical inclusion embedded in an homogeneous matrix. As shown by Eshelby (1957), the stress and strain fields are uniform in the spherical inclusion and can be determined using the

Eshelby inclusion solution. With this solution, the constrained compliance tensor $\mathbf{U}^{(\alpha)}$ can be readily derived. More specifically, the macroscopic stress $\overline{\boldsymbol{\sigma}}$ and strain $\overline{\boldsymbol{\varepsilon}}$ applied to the RVE are taken to be the volume averages of stress and strain in all the grains, respectively. They are related by

$$\overline{\boldsymbol{\sigma}} = \overline{\mathbf{L}}\overline{\boldsymbol{\varepsilon}},\ \overline{\boldsymbol{\varepsilon}} = \overline{\mathbf{M}}\overline{\boldsymbol{\sigma}} \tag{8}$$

where $\overline{\mathbf{L}}$ and $\overline{\mathbf{M}}$ are respectively the effective elastic stiffness and compliance tensor of the homogeneous RVE, such that $\overline{\mathbf{M}} = \overline{\mathbf{L}}^{-1}$. When the RVE is subjected to the macroscopic strain, $\overline{\boldsymbol{\varepsilon}}$, the Eshelby inclusion solution (Qu and Cherkaoui, 2006) shows that the uniform strain $\boldsymbol{\varepsilon}^{(\alpha)}$ in the spherical grain inclusion is given by

$$\boldsymbol{\varepsilon}^{(\alpha)} = \mathbf{T}^{(\alpha)}\overline{\boldsymbol{\varepsilon}} \tag{9}$$

where the global strain concentration tensor $\mathbf{T}^{(\alpha)}$ (Qu and Cherkaoui, 2006) is given by

$$\mathbf{T}^{(\alpha)} = \left[\mathbf{I} + \mathbf{S}^{(\alpha)}\overline{\mathbf{L}}^{-1}\left(\mathbf{L}^{(\alpha)} - \overline{\mathbf{L}}\right)\right]^{-1} \tag{10}$$

In Eq. (10), $\mathbf{I}$ is the fourth rank identify tensor and $\mathbf{S}^{(\alpha)}$ is the Eshelby inclusion tensor of a spherical grain inclusion embedded in a matrix with the elastic stiffness tensor of $\overline{\mathbf{L}}$. From Eqs. (8) and (9), the strain $\boldsymbol{\varepsilon}^{(\alpha)}$ in the grain α can be expressed in terms of the macroscopic stress $\overline{\boldsymbol{\sigma}}$ as

$$\boldsymbol{\varepsilon}^{(\alpha)} = \mathbf{U}^{(\alpha)}\overline{\boldsymbol{\sigma}} \tag{11}$$

where the grain compliance tensor $\mathbf{U}^{(\alpha)}$ is given by

$$\mathbf{U}^{(\alpha)} = \mathbf{T}^{(\alpha)}\overline{\mathbf{M}} \tag{12}$$

To derive the solution of diffraction elastic constants from $\mathbf{U}^{(\alpha)}$, one needs to provide the solution of $\overline{\mathbf{L}}$ from the given single crystal elastic constants. In this work, we use the self-consistent method (Qu and Cherkaoui, 2006) to determine $\overline{\mathbf{L}}$, as shown in Section 4.

4. Constrained compliance tensor U in a cubic polycrystal

From the grain compliance tensor $\mathbf{U}^{(\alpha)}$ given in Section 3, we obtain a general solution of the diffraction elastic constants for an elastically isotropic polycrystal with cubic crystal symmetry. Using the index notation, the components of $\mathbf{L}^{(\alpha)}$ can be expressed in terms of the local crystal basis as (Qu and Cherkaoui, 2006)

$$L^{(\alpha)}_{ijkl} = C_{12}\delta_{ij}\delta_{kl} + C_{44}\left(\delta_{ik}\delta_{jl} + \delta_{il}\delta_{jk}\right) + (C_{11} - C_{12} - 2C_{44})d_{ijkl} \tag{13}$$

where C_{11}, C_{12} and C_{44} are the single crystal elastic constants of cubic crystals, δ_{ij} is the Kronecker delta and the non-zero components of d_{ijkl} are $d_{1111} = d_{2222} = d_{3333} = 1$. As shown by Qu and Cherkaoui (2006), it is helpful to introduce a symbolic representation for the fourth-order tensors involved, so as to facilitate a convenient algebraic operation for these tensors, including addition, subtraction, multiplication, and inverse. Specifically, the components of $\mathbf{L}^{(\alpha)}$ can be equivalently written as

$$L^{(\alpha)}_{ijkl} = (3\eta_1 - 2\eta_2)\frac{1}{3}\delta_{ij}\delta_{kl} + 2\eta_3\frac{1}{2}\left(\delta_{ik}\delta_{jl} + \delta_{il}\delta_{jk}\right) + (2\eta_2 - 2\eta_3)d_{ijkl} \tag{14}$$

where $3\eta_1 = C_{11} + 2C_{12}$, $2\eta_2 = C_{11} - C_{12}$ and $2\eta_3 = 2C_{44}$. Then the fourth-order tensor $\mathbf{L}^{(\alpha)}$ in Eq. (14) can be written symbolically as (Hutchinson, 1970)

$$\mathbf{L}^{(\alpha)} = (3\eta_1, 2\eta_2, 2\eta_3) \tag{15}$$

We consider a polycrystal having a random distribution of grain orientations and thus an isotropic elasticity tensor $\overline{\mathbf{L}}$. With the same symbolic notation, $\overline{\mathbf{L}}$ and its corresponding compliance tensor $\overline{\mathbf{M}}$ are respectively written as

$$\overline{\mathbf{L}} = \left(3\overline{K}, 2\overline{\mu}, 2\overline{\mu}\right) \text{ and } \overline{\mathbf{M}} = \left(\frac{1}{3\overline{K}}, \frac{1}{2\overline{\mu}}, \frac{1}{2\overline{\mu}}\right) \tag{16}$$

where $\overline{K}$ is the effective bulk modulus and $\overline{\mu}$ is the effective shear modulus of an elastically isotropic polycrystal. The equations for $\overline{K}$ and $\overline{\mu}$ from the self-consistent method (Hutchinson, 1970) are given by

$$\overline{K} = \frac{1}{3}(C_{11} + 2C_{12}) \tag{17}$$

$$8\overline{\mu}^3 + (5C_{11} + 4C_{12})\overline{\mu}^2 - C_{44}(7C_{11} - 4C_{12})\overline{\mu} - C_{44}(C_{11} - C_{12})(C_{11} + 2C_{12}) = 0 \tag{18}$$

Given the single crystal elastic constants, one can calculate $\overline{K}$ from Eq. (17) and $\overline{\mu}$ by solving Eq. (18). On the other hand, the Eshelby inclusion tensor for a spherical inclusion in an elastically isotropic matrix can be written symbolically as (Qu and Cherkaoui, 2006)

$$\mathbf{S}^{(\alpha)} = \left(3\overline{\gamma}, 2\overline{\delta}, 2\overline{\delta}\right) \tag{19}$$

where

$$\overline{\gamma} = \frac{\overline{K}}{3\overline{K} + 4\overline{\mu}} \text{ and } \overline{\delta} = \frac{3\overline{K} + 6\overline{\mu}}{15\overline{K} + 20\overline{\mu}} \tag{20}$$

In addition, the fourth-order identity tensor is $\mathbf{I} = (1, 1, 1)$. Our symbolic calculations of $\mathbf{T}^{(\alpha)}$ based on Eq. (10) and $\mathbf{U}^{(\alpha)}$ based on Eq. (12) yield

$$\mathbf{U}^{(\alpha)} = \left(\frac{1}{3\left[\overline{K} + \overline{\gamma}\left(3\eta_1 - 3\overline{K}\right)\right]}, \frac{1}{2\left[\overline{\mu} + \overline{\delta}(2\eta_2 - 2\overline{\mu})\right]}, \frac{1}{2\left[\overline{\mu} + \overline{\delta}(2\eta_3 - 2\overline{\mu})\right]} \right) \tag{21}$$

To proceed further, we represent $\mathbf{U}^{(\alpha)}$ symbolically as

$$\mathbf{U}^{(\alpha)} = (3a, 2b, 2c) \tag{22}$$

where $3a$, $2b$ and $2c$ correspond to the respective component of $\mathbf{U}^{(\alpha)}$ in Eq. (21). By comparing Eqs. (14) and (15), we rewrite $\mathbf{U}^{(\alpha)}$ in Eq. (22) as

$$U_{ijkl}^{(\alpha)} = (3a - 2b)\frac{1}{3}\delta_{ij}\delta_{kl} + 2c\frac{1}{2}\left(\delta_{ik}\delta_{jl} + \delta_{il}\delta_{jk}\right) + (2b - 2c)d_{ijkl} \tag{23}$$

The solution of $U_{ijkl}^{(\alpha)}$ in Eq. (23) is used to determine lattice strains and diffraction elastic constants in Sections 5-7; it can be also used to calculate grain-level stresses for the study of progressive yielding in different grain families (Chen et al., 2019). It should be emphasized that the solution of $U_{ijkl}^{(\alpha)}$ applies to a random orientation of grains. Consideration of crystallographic textured polycrystals is beyond the scope of this work.

5. Diffraction elastic constants along LD

Consider a $\{hkl\}$ grain family along LD in an RVE (Fig. 1b). The grains in this family are numbered as 1, ... α, ... N. In the local crystal basis of grain α, the component of the unit vector $\mathbf{n}$ along the $[hkl]$ direction can be expressed as

$$\mathbf{n} = (n_1, n_2, n_3) = (h, k, l)/\sqrt{h^2 + k^2 + l^2} \tag{24}$$

From Eqs. (7) and (23), the diffraction elastic constant for the $\{hkl\}$ grain family along LD is derived as

$$\frac{1}{E_{\mathrm{LD}}^{hkl}} = \frac{1}{N}\sum_{\alpha=1}^{N}\left[\frac{3a - 2b}{3}n_i n_i n_k n_k + 2c n_i n_i n_j n_j + 2(b - c)\sum_{i}^{3}(n_i)^4\right] \tag{25}$$

With $n_i n_i = 1$, substitution of Eq. (24) into Eq. (25) yields

$$\frac{1}{E_{\mathrm{LD}}^{hkl}} = \frac{3a + 4b}{3} - 4(b - c)\Gamma \tag{26}$$

where the orientation index parameter Γ is defined as

$$\Gamma = \frac{h^2k^2 + l^2k^2 + h^2l^2}{\left(h^2 + k^2 + l^2\right)^2} \tag{27}$$

This orientation parameter varies between 0 and 1/3 to cover all the grain families with random orientations, and they are 0, 19/121, 1/4 and 1/3 for the representative grain families of {200}, {311}, {220} and {111}, respectively. Eq. (26) reveals a linear dependence of $1/E_{\mathrm{LD}}^{hkl}$ on Γ, which has been previously shown by Bollenrath et al. (1967). In addition, Eq. (26) shows that the linear dependence of $1/E_{\mathrm{LD}}^{hkl}$ on Γ is dictated by $b - c$. Since $4(b - c) = \overline{\delta}(\eta_3 - \eta_2)/\{[\overline{\mu} + \overline{\delta}(2\eta_2 - 2\overline{\mu})][\overline{\mu} + \overline{\delta}(2\eta_3 - 2\overline{\mu})]\}$, the sign of $b - c$ is determined predominantly by $\eta_3 - \eta_2$ and thus by the anisotropy ratio $A = 2C_{44}/(C_{11} - C_{12}) = \eta_3/\eta_2$. Hence, Eq. (26) indicates that if $A > 1$, then $b - c > 0$ and thus E_{LD}^{hkl} increases withΓ, and vice versa. For example, $E_{\mathrm{LD}}^{111} > E_{\mathrm{LD}}^{200}$ for FCC Cu, because of $A = 3.21$, while $E_{\mathrm{LD}}^{111} < E_{\mathrm{LD}}^{200}$ for BCC Nb, due to $A = 0.49$. This analysis relates the anisotropy ratio A to the relative magnitude of E_{LD}^{111} and E_{LD}^{200}, a factor that strongly influences the progressive yielding responses during loading as well as the residual stress responses after unloading in different grain families (Dye et al., 2001).

Using the analytic solution of Eq. (26), we calculated the diffraction elastic constants for various cubic polycrystals, with the experimental values of single crystal elastic constants from Simmons and Wang (1971), which are also provided in the Appendix. Table 1 lists the numerical results of the diffraction elastic constants along LD for 26 representative elastically isotropic polycrystals with FCC, BCC and DC crystal symmetries (as indicated in the Appendix).

To validate the present analytic solution and associated calculations of diffraction elastic constants, we compared our numerical results of FCC Cu and stainless steel (SS) 316L with literature data. Table 2 shows that our results of diffraction elastic constants along LD closely match those by Clausen et al. (1998), who used Kröner's self-consistent solution and the same sets of single crystal elastic constants as ours. In addition, Table 2 shows that our results of diffraction elastic constants along LD for SS 316L reasonably agree with SXRD measurements (Chen et al., 2019).

Table 1
Diffraction elastic constants E_{LD}^{hkl} along LD (in GPa).

	E_{LD}^{200}	E_{LD}^{220}	E_{LD}^{111}	E_{LD}^{311}
Ag	65.30	88.43	100.27	78.14
Al	67.09	71.29	72.80	69.67
Au	63.55	84.69	95.25	75.36
Cu	101.15	139.06	158.91	122.05
Ir	491.12	554.66	579.65	529.19
Ni	183.74	237.86	263.76	214.38
Pb	18.59	26.97	31.74	23.10
Pd	107.11	142.53	160.18	126.92
Pt	159.41	182.98	192.47	173.45
Cr	298.59	267.89	259.02	278.54
Fe	175.18	224.29	247.40	203.11
K	2.50	3.96	4.92	3.25
Li	7.43	12.4	15.97	9.93
Mo	335.10	325.04	321.81	328.71
Na	4.41	7.56	9.92	5.98
Nb	127.25	100.46	93.87	109
Ta	166.76	190.41	199.86	180.87
V	136.79	126.33	123.19	130.03
W	408.65	410.07	410.55	409.54
C	963.66	1037.68	1064.95	1008.86
Ge	117.23	135.63	143.12	128.15
Si	147.69	168.02	176.10	159.84
CuZn	70.13	116.95	150.42	93.69
Cu_3Au	103.15	133.9	148.67	120.54
NiAl	144.94	200.23	229.4	175.35
SS 316L	149.25	212.69	247.81	183.66

Table 2
Comparison of the present model predictions of E_{LD}^{hkl} (in GPa) along LD with those by Clausen et al. (1998) for Cu and SS 316L as well as with SXRD measurements for SS 316L (Chen et al., 2019).

	E_{LD}^{200}	E_{LD}^{220}	E_{LD}^{111}	E_{LD}^{311}
Cu (this work)	101.2	139.1	158.9	122.1
Cu (Clausen et al., 1998)	101.5	138.7	158.0	121.8
SS 316L (this work)	149.3	212.7	247.8	183.7
SS 316L (Clausen et al., 1998)	149.8	212.0	246.2	183.2
SS 316L (Chen et al., 2019)	139.1	219.1	264.1	179.6

6. Diffraction elastic constants along TD

To extend the method in Section 5 for determining the diffraction elastic constants along TD, we note that the corresponding unit vector along LD is not unique. Hence, one needs to account for a set of LD vectors that are perpendicular to a given TD. Consider a $\{hkl\}$ grain family along TD in an RVE (Fig. 1b). The grains in this family are numbered as 1, ... β, ... N. In the local crystal basis of grain β, the component of the unit vector $\mathbf{m}$ along the $[hkl]$ direction can be expressed as

$$\mathbf{m} = (m_1, m_2, m_3) = (h, k, l)\Big/\sqrt{h^2 + k^2 + l^2} \tag{28}$$

As noted above, the unit vector along LD for grain β, denoted as $\mathbf{n}^{(\beta)}$, can be any vector perpendicular to $\mathbf{m}$. Without loss of generality, we can express $\mathbf{n}^{(\beta)}$ using a single variable θ. Specifically, we introduce the orthonormal basis vectors $\mathbf{p}$ and $\mathbf{q}$ in the plane perpendicular to $\mathbf{m}$

$$\begin{aligned}\mathbf{p} &= (p_1, p_2, p_3) = (-k, h, 0)/\sqrt{h^2 + k^2}\\ \mathbf{q} &= (q_1, q_2, q_3) = \left(hl, kl, -h^2 - k^2\right)\Big/\sqrt{\left(h^2 + k^2\right)\left(h^2 + k^2 + l^2\right)}\end{aligned} \tag{29}$$

While there are many ways of choosing a pair of $\mathbf{p}$ and $\mathbf{q}$, we first select a unit vector $\mathbf{p}$ perpendicular to $\mathbf{m}$, and then determine $\mathbf{q}$ by the cross product of $\mathbf{p}$ and $\mathbf{m}$. Since $\mathbf{n}^{(\beta)}$ associated with grain β lies in the plane spanned by $\mathbf{p}$ and $\mathbf{q}$, we can write $\mathbf{n}^{(\beta)}$ as

$$\mathbf{n}^{(\beta)} = \mathbf{p}\cos\theta^{(\beta)} + \mathbf{q}\sin\theta^{(\beta)} \tag{30}$$

where $\theta^{(\beta)}$ denotes the angle between $\mathbf{n}^{(\beta)}$ and $\mathbf{p}$. By this construction, $\mathbf{n}^{(\beta)}$ is perpendicular to $\mathbf{m}$ automatically.

Similar to $\varepsilon_{\mathrm{LD}}^{(\alpha)}$ in Eq. (3), the lattice strain along TD in grain β can be calculated as

$$\varepsilon_{\mathrm{TD}}^{(\beta)} = \varepsilon_{ij}^{(\beta)} m_i m_j \tag{31}$$

Substitution of Eq. (1) (replacing α by β) into Eq. (31) yields

$$\varepsilon_{\mathrm{TD}}^{(\beta)} = \sigma_0 U_{ijkl}^{(\beta)} m_i m_j n_k^{(\beta)} n_l^{(\beta)} \tag{32}$$

With $n_i m_i = 0$ and Eq. (30), Eq. (32) can be expressed as

$$\frac{\varepsilon_{\mathrm{TD}}^{(\beta)}}{\sigma_0} = \frac{3a-2b}{3} + \sum_{i=1}^{3} \left(p_i \cos\theta^{(\beta)} + q_i \sin\theta^{(\beta)}\right)^2 m_i^2 \tag{33}$$

The average lattice strain $\overline{\varepsilon}_{\mathrm{TD}}$ in the $\{hkl\}$ grain family along TD is, therefore, given by

$$\overline{\varepsilon}_{\mathrm{TD}} = \frac{1}{N} \sum_{\beta=1}^{N} \varepsilon_{\mathrm{TD}}^{(\beta)} \tag{34}$$

The diffraction elastic constant along TD is defined as

$$\frac{1}{E_{\mathrm{TD}}^{hkl}} = \frac{\overline{\varepsilon}_{\mathrm{TD}}}{\sigma_0} = \frac{1}{\sigma_0 N} \sum_{\beta=1}^{N} \varepsilon_{\mathrm{TD}}^{(\beta)} \tag{35}$$

Since σ_0 and $\varepsilon_{\mathrm{TD}}^{(\beta)}$ have opposite signs by virtue of Poisson's effect, E_{TD}^{hkl} defined in Eq. (35) is negative. Substituting Eq. (33) into Eq. (35) yields

$$\frac{1}{E_{\mathrm{TD}}^{hkl}} = \frac{1}{N} \sum_{\beta=1}^{N} \left[\frac{3a-2b}{3} + 2(b-c) \sum_{i=1}^{3} \left(p_i \cos\theta^{(\beta)} + q_i \sin\theta^{(\beta)}\right)^2 m_i^2 \right] \tag{36}$$

For a sufficiently large RVE, the $\{hkl\}$ grain family along TD should contain a sufficient number of randomly oriented grains with $\mathbf{n}^{(\beta)}$ in the plane spanned by $\mathbf{p}$ and $\mathbf{q}$. Hence, one can change the summation over β grains in Eq. (36) to the integration over θ from 0 to 2π, and then use Eq. (30) to obtain

$$\begin{aligned} \frac{1}{E_{\mathrm{TD}}^{hkl}} &= \frac{1}{\sigma_0 2\pi} \int_0^{2\pi} \varepsilon_{\mathrm{TD}}(\theta) d\theta \\ &= \frac{3a-2b}{3} + 2(b-c) \frac{1}{2\pi} \int_0^{2\pi} \sum_{i=1}^{3} (p_i \cos\theta + q_i \sin\theta)^2 m_i^2 d\theta \\ &= \frac{3a-2b}{3} + (b-c) \sum_{i=1}^{3} \left(p_i^2 + q_i^2\right) m_i^2 \end{aligned} \tag{37}$$

Substituting Eqs. (28) and (29) into Eq. (37), we obtain

$$\frac{1}{E_{\mathrm{TD}}^{hkl}} = \frac{3a-2b}{3} + 2(b-c)\Gamma \tag{38}$$

where the orientation index parameter Γ is defined in Eq. (27).

Similar to E_{LD}^{hkl}, we calculated the numerical values of E_{TD}^{hkl} using Eq. (38) and single crystal elastic constants in the Appendix. Table 3 lists the numerical results of E_{TD}^{hkl} for 26 representative elastically isotropic polycrystals with FCC, BCC and DC crystal symmetries.

7. Diffraction elastic constants along any Q direction

We further extend the method in Section 6 to derive the solution of diffraction elastic constants along the direction of any diffraction vector **Q** (see Fig. 1a). Consider a $\{hkl\}$ grain family along the **Q** direction in an RVE. The grains in this family are numbered as 1, ... γ, ... N. The orientation of these grains can be represented by a single variable $\theta^{(\gamma)}$ and three orthogonal unit vectors as shown in Fig. 2,

$$\begin{aligned} \mathbf{Q} &= (Q_1, Q_2, Q_3) = (h, k, l)/\sqrt{h^2+k^2+l^2} \\ \mathbf{p} &= (p_1, p_2, p_3) = (-k, h, 0)/\sqrt{h^2+k^2} \\ \mathbf{q} &= (q_1, q_2, q_3) = \left(hl, kl, -h^2-k^2\right)/\sqrt{\left(h^2+k^2\right)\left(h^2+k^2+l^2\right)} \end{aligned} \tag{39}$$

In Eq. (39), the components of **Q**, **p** and **q** are all expressed in the local crystal basis of grain γ.

For the $\{hkl\}$ grain family along the **Q** direction, the constituent grains must have a constant angle between **Q** and the loading direction **n**, such that $\mathbf{n}^{(\gamma)}$ associated with grain γ can be expressed as

$$\mathbf{n}^{(\gamma)} = \mathbf{Q}\cos\varphi + \left(\mathbf{p}\cos\theta^{(\gamma)} + \mathbf{q}\sin\theta^{(\gamma)}\right)\sin\varphi \tag{40}$$

Table 3
Magnitude of diffraction elastic constants $|E_{\mathrm{TD}}^{hkl}|$ along TD (in GPa).

	$\lvert E_{\mathrm{TD}}^{200}\rvert$	$\lvert E_{\mathrm{TD}}^{220}\rvert$	$\lvert E_{\mathrm{TD}}^{111}\rvert$	$\lvert E_{\mathrm{TD}}^{311}\rvert$
Ag	165.35	247.21	296.06	208.77
Al	189.76	206.98	213.44	200.22
Au	144.77	202.29	233.17	176.24
Cu	268.3	420.22	517.98	347.12
Ir	1824.28	2317.3	2546.73	2105.67
Ni	556.41	848.88	1029.22	710.07
Pb	43.16	67.52	83.16	55.81
Pd	262.84	378.12	442.87	325.09
Pt	392.63	466.65	497.94	436.08
Cr	1722.85	1294.79	1195.75	1426.61
Fe	538.86	812.42	977.91	683.39
K	6.50	12.52	18.11	9.31
Li	18.67	37.64	56.92	27.32
Mo	1168.72	1108.85	1090.23	1130.38
Na	12.17	28.57	51.86	19.03
Nb	343.44	252.56	232.08	280.12
Ta	471.74	572.27	616.03	530.25
V	387.47	346.78	335.06	360.88
W	1456.48	1465.52	1468.55	1462.14
C	8391.01	12,171.11	14,321.73	10,424.59
Ge	489.97	683.84	787.73	596.12
Si	590.51	778.95	871.67	696.31
CuZn	175.65	352.21	529.7	256.37
Cu_3Au	264.74	375.35	436.09	324.87
NiAl	408.88	669.73	850.62	541.3
SS 316L	433.18	763.86	1024.57	594.95

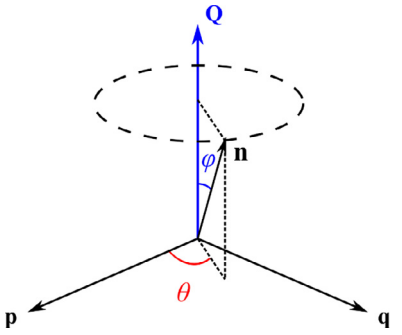

Fig. 2. In the coordinate system spanned by the orthonormal vectors {**Q**, **p**, **q**}, the dashed-line circle represents all the unit vectors **n** that form a constant angle φ with the diffraction vector **Q**.

where φ denotes the angle between **Q** and $\mathbf{n}^{(\gamma)}$, and $\theta^{(\gamma)}$ denotes the angle between **p** and the vector component of $\mathbf{n}^{(\gamma)}$ resolved in the plane of **p** and **q**.

The normal strain along **Q** for grain γ, denoted as $\varepsilon_{\mathrm{Q}}^{(\gamma)}$, is given by

$$\varepsilon_{\mathrm{Q}}^{(\gamma)} = \sigma_0 U_{ijkl}^{(\gamma)} Q_i Q_j n_k^{(\gamma)} n_l^{(\gamma)} \tag{41}$$

Substitution of Eqs. (22), (39) and (40) into Eq. (41) yields

$$\begin{aligned}\frac{\varepsilon_{\mathrm{Q}}^{(\gamma)}}{\sigma_0} &= \frac{3a-2b}{3} + 2c\cos^2\varphi + 2(b-c)(1-2\Gamma)\cos^2\varphi \\ &\quad + 2(b-c)\sum_{i=1}^{3} Q_i^2\left[2Q_i\left(p_i\cos\theta^{(\gamma)} + q_i\sin\theta^{(\gamma)}\right)\sin\varphi\cos\varphi + \left(p_i\cos\theta^{(\gamma)} + q_i\sin\theta^{(\gamma)}\right)^2\sin^2\varphi\right]\end{aligned} \tag{42}$$

The average lattice strain $\bar{\varepsilon}_{\mathrm{Q}}$ in the {*hkl*} grain family along **Q** is given by

$$\bar{\varepsilon}_{\mathrm{Q}} = \frac{1}{N}\sum_{\gamma=1}^{N} \varepsilon_{\mathrm{Q}}^{(\gamma)} \tag{43}$$

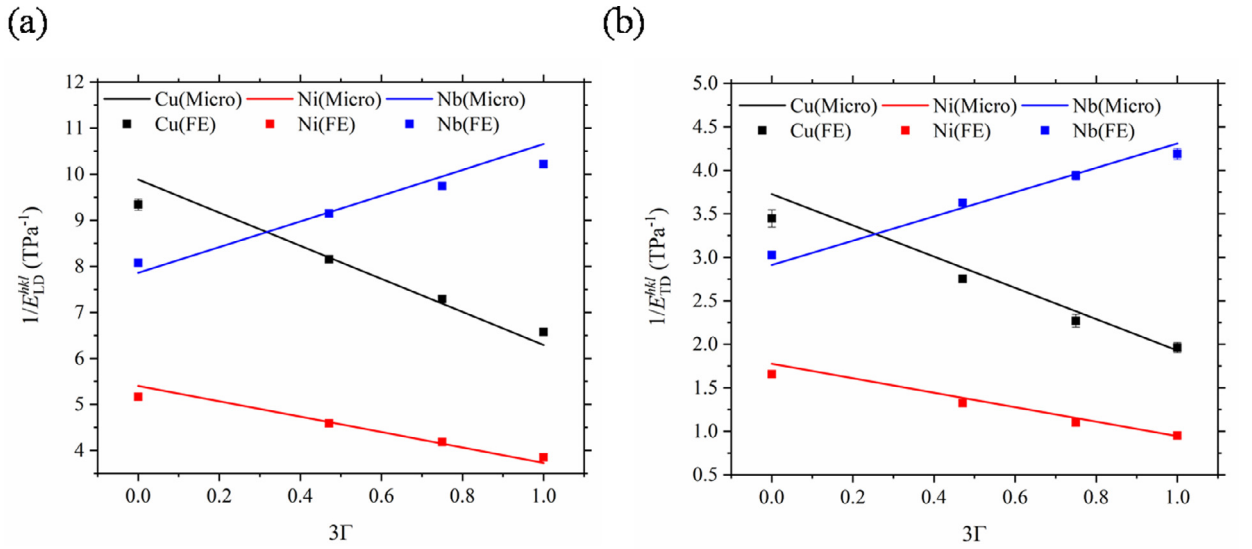

Fig. 3. Plot of the reciprocal of diffraction elastic constant $1/E^{hkl}$ as a function of orientation parameter Γ along (a) LD and (b) TD for FCC Cu, Ni and BCC Nb. The solid lines represent the micromechanics (Micro) solutions, and the squares the finite element (FE) simulation results for the representative grain families of {200}, {311}, {220} and {111}, with their respective 3Γ values of 0, 57/121, 3/4 and 1. Each FE data point is the average of results from 10 FE polycrystal models with different random grain orientations; small error bars indicate negligible standard deviations.

The diffraction elastic constant along **Q** is, therefore, defined as

$$\frac{1}{E^{hkl}_{Q}} = \frac{\bar{\varepsilon}_{Q}}{\sigma_0} = \frac{1}{\sigma_0 N}\sum_{\gamma=1}^{N}\varepsilon_{Q}^{(\gamma)} \tag{44}$$

With a sufficient number of grains, one can change the summation over γ in Eq. (44) to the integration over θ from 0 to 2π. Substituting Eq. (42) into Eq. (44), we obtain the general solution of diffraction elastic constant E^{hkl}_{Q} for any diffraction vector **Q**.

$$\begin{aligned}\frac{1}{E^{hkl}_{Q}} &= \frac{1}{\sigma_0 2\pi}\int_0^{2\pi}\varepsilon_{Q}(\theta)d\theta \\ &= \frac{3a-2b}{3} + 2c\cos^2\varphi + 2(b-c)(1-2\Gamma)\cos^2\varphi + (b-c)\sum_{i=1}^{3}Q_i^2\left(p_i^2+q_i^2\right)\sin^2\varphi \\ &= \frac{3a-2b}{3} + 2b\cos^2\varphi + 2(b-c)\left(\sin^2\varphi - 2\cos^2\varphi\right)\Gamma\end{aligned} \tag{45}$$

This expression is reduced to Eq. (26) when $\varphi = 0^\circ$ and Eq. (38) when $\varphi = 90^\circ$. Hence the solutions of E^{hkl}_{LD} and E^{hkl}_{TD} are two special cases of the general solution of E^{hkl}_{Q} for any diffraction vector **Q**.

8. Validation by finite element simulations

To validate our micromechanics solutions, we performed polycrystal elasticity finite element simulations for FCC Cu, Ni, and BCC Nb using the commercial finite element program ABAQUS/Explicit (2016). The constitutive model of the anisotropic linear elasticity of single crystal grains was implemented via a user material subroutine (Chen et al., 2019). For finite element simulations, we constructed a "texture-free" polycrystal model consisting of 8000 cubic elements, where each element represents a cubic-symmetry grain with random orientation. During a finite element simulation of uniaxial tensile deformation, the lattice strain in each {*hkl*} grain family was determined by averaging the elastic strain of grains with their respective [*hkl*] direction along LD or TD (within a deviation of ±5°). Then we calculated the diffraction elastic constant E^{hkl} by the ratio of the applied tensile stress and corresponding lattice strain.

Fig. 3 shows the diffraction elastic constants of Cu, Ni, and Nb along LD (Fig. 3a) and TD (Fig. 3b) calculated from the micromechanics solutions (i.e., Eq. (26) for LD and Eq. (38) for TD) as well as from the polycrystal elasticity finite element simulations. The micromechanics solutions (solid lines) are plotted as a function of the orientation index parameter 3Γ covering all the possible {*hkl*} grain families for a polycrystal with random grain orientations. The polycrystal elasticity finite element simulation results (squares) are given for the {200}, {311}, {220} and {111} grain families. For each family, we used 10 finite element polycrystal models with different random grain orientations, so as to obtain the mean value and standard

deviation of $1/E^{hkl}$. It is seen that the finite element results are in good agreement with the micromechanics solution, despite small differences in the numerical results of $1/E^{hkl}$ between the two methods. These differences may arise from several approximations used in the micromechanics solution, including the self-consistent method of polycrystal homogenization and the spherical grain shape, as well as the use of a single element to represent each grain in the finite element simulations.

As shown in Fig. 3, $1/E^{hkl}$ is linearly dependent on 3Γ. This is predicted by the micromechanics solutions, i.e., Eq. (26) for LD and Eq. (38) for TD. As discussed earlier, the slope of the $1/E^{hkl}$ versus 3Γ curve is dictated by the sign of $b-c$, which is further controlled by the anisotropy ratio A, with $A = 1.0$ for isotropic elasticity, 3.21 for Cu, 2.57 for Ni and 0.49 for Nb. As listed in the Appendix, the A values are greater than 1 for most cubic polycrystals, so that $b-c<0$. As a result, the slopes of both the $1/E^{hkl}_{\mathrm{LD}}$ versus 3Γ and the $1/E^{hkl}_{\mathrm{TD}}$ versus 3Γ curves are negative. In contrast, the positive slope for Nb is a result of $b-c>0$. Among 26 cubic polycrystals in the Appendix, Cr, Mo, and V also have $A<1$ and thus should have positive slopes for their respective $1/E^{hkl}$ versus 3Γ curves. In addition, the slopes of the $1/E^{hkl}_{\mathrm{LD}}$ versus 3Γ and the $1/E^{hkl}_{\mathrm{TD}}$ versus 3Γ curves for Cu are larger than the corresponding ones for Ni because of the higher elastic anisotropy of Cu.

9. Concluding remarks

We have obtained a general analytic solution of the grain-level lattice strains and diffraction elastic constants for elastically isotropic polycrystals using a self-consistent micromechanics model. This solution is applicable to a broad class of "texture-free" polycrystals with cubic crystal symmetry and only requires an input of the three independent elastic constants of a cubic crystal. It reveals direct linear relationships between the reciprocal of the diffraction elastic constant and the orientation index parameter, as given by Eq. (26) for the tensile loading direction, Eq. (38) for the transverse direction, and Eq. (45) for the direction of any diffraction vector. Our solution procedure employs the components of related vectors and tensors resolved in the local crystal basis, such that it can be readily understood and applied. For example, this approach can be taken to obtain the related results such as resolved shear stresses on dislocation slip systems for the study of progressive yielding in different grain families (Chen et al., 2019). From a straightforward numerical implementation of this solution by MATLAB, we have calculated diffraction elastic constants for 26 representative cubic polycrystals. The results agree closely with modeling and experimental results in the literature as well as with our polycrystal elasticity finite element simulations.

Theoretical predictions of grain-level lattice strains and diffraction elastic constants complement *in situ* synchrotron X-ray and neutron diffraction experiments. They can be directly compared with experimental measurements of diffraction elastic constants, and also can be used for analysis of microscale residual stresses (Hu et al., 2016) and progressive yielding (Chen et al., 2019; Wang et al., 2018b). We expect these predictions will facilitate high-throughput and data-analytics studies of the mechanical behavior of polycrystalline materials with complex compositions and microstructures, such as high-entropy alloys (Wang et al., 2018a; Wu et al., 2014), additively manufactured alloys (Brown et al., 2017; Chen et al., 2019; Wang et al., 2018b), heterogeneous nanostructured metals and alloys (Ma and Zhu, 2017; Wang et al., 2010), and others. However, one should bear in mind the assumptions used in the present model, including equiaxed grains, absence of textures, and lack of pore defects. Our solutions are applicable to cases where these assumptions can be used appropriately.

The analytic solution in this paper is derived for elastically isotropic polycrystals with cubic crystal symmetry. The present method can be extended to other types of elastically isotropic polycrystals with lower crystal symmetries, such as hexagonal close-packed and monoclinic crystals that have been studied by diffraction experiments (Kumar et al., 2018; Stebner et al., 2013). For these types of polycrystals, the constrained compliance tensor $\mathbf{U}$ cannot be expressed in a highly compact form as given in Eq. (21) for cubic polycrystals. Hence the corresponding analytic solutions of diffraction elastic constants become more complex and are only partially provided by Behnken and Hauk (1986). Additional effort is needed to obtain the complete analytic solutions by extending the current method. We hope to obtain and report these results in the near future.

Declaration of Competing Interest

The authors declare that they have no known competing financial interests or personal relationships that could have appeared to influence the work reported in this paper.

CRediT authorship contribution statement

Yin Zhang: Conceptualization, Methodology, Software, Writing - original draft. **Wen Chen:** Writing - review & editing. **David L. McDowell:** Supervision, Writing - review & editing. **Y. Morris Wang:** Supervision, Writing - review & editing. **Ting Zhu:** Supervision, Conceptualization, Writing - original draft, Writing - review & editing.

Acknowledgments

TZ and DLM acknowledge support from the Office of Naval Research under grant number N00014-18-1-2784. The work at Lawrence Livermore National Laboratory was performed under the auspices of the US Department of Energy under contract number DE-AC52-07NA27344.

Supplementary materials

Supplementary material associated with this article can be found, in the online version, at doi:10.1016/j.jmps.2020.103899.

Appendix

Table A1.

Table A1
Elastic properties of cubic polycrystals. The single crystal elastic constants of C_{11}, C_{12} and C_{44} (in GPa) are taken from Simmons and Wang (1971), except for those of SS 316L from Clausen et al. (1998). The effective elastic consonants $\bar{K}$ and $\bar{\mu}$ (in GPa) for elastically isotropic polycrystals are calculated from Eq. (17) and Eq. (18), respectively. The anisotropy ratio A is calculated by $A = 2C_{44}/(C_{11} - C_{12})$.

Material	Structure	C_{11}	C_{12}	C_{44}	$\bar{K}$	$\bar{\mu}$	A
Ag	FCC	124.00	93.40	46.10	103.60	30.20	3.01
Al	FCC	107.30	60.90	28.30	76.37	26.15	1.22
Au	FCC	192.90	163.80	41.50	173.50	27.89	2.85
Cu	FCC	168.40	121.40	75.40	137.07	48.17	3.21
Ir	FCC	580.00	242.00	256.00	354.67	216.97	1.51
Ni	FCC	246.50	147.30	124.70	180.37	86.90	2.51
Pb	FCC	49.50	42.30	14.90	44.70	8.79	4.14
Pd	FCC	227.10	176.00	71.70	193.03	48.28	2.81
Pt	FCC	346.70	250.70	76.50	282.70	63.69	1.59
Cr	BCC	339.80	58.60	99.00	152.33	113.89	0.70
Fe	BCC	231.40	134.70	116.40	166.93	82.45	2.41
K	BCC	4.14	3.31	2.63	3.59	1.33	6.34
Li	BCC	13.50	11.44	8.78	12.13	4.05	8.52
Mo	BCC	440.80	172.40	121.70	261.87	126.56	0.91
Na	BCC	6.15	4.96	5.92	5.36	2.56	9.95
Nb	BCC	240.20	125.60	28.20	163.80	37.64	0.49
Ta	BCC	260.20	154.50	82.60	189.73	69.23	1.56
V	BCC	228.00	118.70	42.60	155.13	47.09	0.78
W	BCC	522.40	204.40	160.80	310.40	160.08	1.01
C	DC	949.00	151.00	521.00	417.00	468.14	1.31
Ge	DC	128.40	48.20	66.70	74.93	54.45	1.66
Si	DC	166.70	64.40	79.80	98.50	66.83	1.56
CuZn	FCC	129.04	109.56	82.45	116.05	38.16	8.47
Cu_3Au	FCC	190.69	138.30	66.31	155.76	46.29	2.53
NiAl	BCC	211.55	143.23	112.11	166.00	70.83	3.28
SS 316L	FCC	204.60	137.70	126.20	160.00	75.64	3.77

References

ABAQUS/Explicit, 2016. User's Manual. SIMULIA, Providence, R.I.

Allen, A.J., Hutchings, M.T., Windsor, C.G., Andreani, C., 1985. Neutron diffraction methods for the study of residual stress fields. Adv. Phys. 34, 445–473.

Behnken, H., Hauk, V., 1986. Calculation of the X-ray elasticity constants (XEC) of the polycrystal from the elastic data of the single-crystal for arbitrary crystal symmetry. Z. Metallkd. 77, 620–626.

Bollenrath, F., Hauk, V., Müller, E.H., 1967. On the calculation of polycrystalline elasticity constants from single crystal data. Z. Metallkd. 58, 76–82.

Brown, D.W., Adams, D.P., Balogh, L., Carpenter, J.S., Clausen, B., King, G., Reedlunn, B., Palmer, T.A., Maguire, M.C., Vogel, S.C., 2017. In situ neutron diffraction study of the influence of microstructure on the mechanical response of additively manufactured 304L stainless steel. Metall. Mater. Trans. A 48, 6055–6069.

Chen, W., Voisin, T., Zhang, Y., Florien, J.-B., Spadaccini, C.M., McDowell, D.L., Zhu, T., Wang, Y.M., 2019. Microscale residual stresses in additively manufactured stainless steel. Nat. Commun. 10, 4338.

Clausen, B., Lorentzen, T., Bourke, M.A.M., Daymond, M.R., 1999. Lattice strain evolution during uniaxial tensile loading of stainless steel. Mater. Sci. Eng. A 259, 17–24.

Clausen, B., Lorentzen, T., Leffers, T., 1998. Self-consistent modelling of the plastic deformation of fcc polycrystals and its implications for diffraction measurements of internal stresses. Acta Mater. 46, 3087–3098.

Daymond, M.R., Bourke, M.A.M., VonDreele, R.B., Clausen, B., Lorentzen, T., 1997. Use of rietveld refinement for elastic macrostrain determination and for evaluation of plastic strain history from diffraction spectra. J. Appl. Phys. 82, 1554–1562.

Daymond, M.R., Tome, C.N., Bourke, M.A.M., 2000. Measured and predicted intergranular strains in textured austenitic steel. Acta Mater. 48, 553–564.

DeWit, R., 1997. Diffraction elastic constants of a cubic polycrystal. J. Appl. Crystallogr. 30, 510–511.

Dye, D., Stone, H.J., Reed, R.C., 2001. Intergranular and interphase microstresses. Curr. Opin. Solid State Mater. Sci. 5, 31–37.

Eshelby, J.D., 1957. The determination of the elastic field of an ellipsoidal inclusion, and related problems. Proc. R. Soc. Lond. Ser. A 241, 376–396.

Gnaupel-Herold, T., Brand, P.C., Prask, H.J., 1998. Calculation of single-crystal elastic constants for cubic crystal symmetry from powder diffraction data. J. Appl. Crystallogr. 31, 929–935.

Holden, T.M., Clarke, A.P., Holt, R.A., 1997. Neutron diffraction measurements of intergranular strains in monel-400. Metall. Mater. Trans. A 28, 2565–2576.

Holden, T.M., Holt, R.A., Clarke, A.P., 1998. Intergranular strains in inconel-600 and the impact on interpreting stress fields in beat steam-generator tubing. Mater. Sci. Eng. A 246, 180–198.

Hommer, G.M., Park, J.-S., Brunson, Z.D., Dahal, J., Kenesei, P., Mashayekhi, A., Almer, J.D., Vignes, J., Lemmer, S.R., Clausen, B., Brown, D.W., Stebner, A.P., 2019. A planar biaxial experiment platform for in situ high-energy diffraction studies. Exp. Mech. 59, 749–774.

Hu, J.N., Chen, B., Smith, D.J., Flewitt, P.E.J., Cocks, A.C.F., 2016. On the evaluation of the Bauschinger effect in an austenitic stainless steel-The role of multi-scale residual stresses. Int. J. Plast. 84, 203–223.
Hutchinson, J.W., 1970. Elastic-plastic behaviour of polycrystalline metals and composites. Proc. R. Soc. Lond. Ser. A 319, 247–272.
Ice, G.E., Budai, J.D., Pang, J.W.L., 2011. The race to X-ray microbeam and nanobeam science. Science 334, 1234–1239.
Kröner, E., 1960. Allgemeine kontinuumstheorie der versetzungen und eigenspannungen. Arch. Ration. Mech. Anal. 4, 273–334.
Kumar, M.A., Clausen, B., Capolungo, L., McCabe, R.J., Liu, W., Tischler, J.Z., Tome, C.N., 2018. Deformation twinning and grain partitioning in a hexagonal close-packed magnesium alloy. Nat. Commun. 9, 4761.
Li, D.-F., O'Dowd, N.P., 2011. On the evolution of lattice deformation in austenitic stainless steels—The role of work hardening at finite strains. J. Mech. Phys. Solids 59, 2421–2441.
Li, R., Xie, Q., Wang, Y.-D., Liu, W., Wang, M., Wu, G., Li, X., Zhang, M., Lu, Z., Geng, C., Zhu, T., 2018. Unraveling submicron-scale mechanical heterogeneity by three-dimensional X-ray microdiffraction. Proc. Natl. Acad. Sci. U.S.A. 115, 483–488.
Ma, E., Zhu, T., 2017. Towards strength–ductility synergy through the design of heterogeneous nanostructures in metals. Mater. Today 20, 323–331.
Margulies, L., Winther, G., Poulsen, H.F., 2001. In situ measurement of grain rotation during deformation of polycrystals. Science 291, 2392–2394.
Pang, J.W.L., Holden, T.M., Mason, T.E., 1998. The development of intergranular strains in a high-strength steel. J. Strain Anal. Eng. 33, 373–383.
Pang, J.W.L., Holden, T.M., Wright, J.S., Mason, T.E., 2000. The generation of intergranular strains in 309H stainless steel under uniaxial loading. Acta Mater. 48, 1131–1140.
Qu, J., Cherkaoui, M., 2006. Fundamentals of Micromechanics of Solids. Wiley, Hoboken, N.J.
Simmons, G., Wang, H., 1971. Single Crystal Elastic Constants and Calculated Aggregate Properties: A Handbook, 2nd ed. Cambridge, Mass., M.I.T. Press, Cambridge, Mass.
Stebner, A.P., Brown, D.W., Brinson, L.C., 2013. Measurement of elastic constants of monoclinic nickel-titanium and validation of first principles calculations. Appl. Phys. Lett. 102, 211908.
Wang, Y., Liu, B., Yan, K., Wang, M., Kabra, S., Chiu, Y.-L., Dye, D., Lee, P.D., Liu, Y., Cai, B., 2018a. Probing deformation mechanisms of a FeCoCrNi high-entropy alloy at 293 and 77K using in situ neutron diffraction. Acta Mater. 154, 79–89.
Wang, Y.M., Ott, R.T., Hamza, A.V., Besser, M.F., Almer, J., Kramer, M.J., 2010. Achieving large uniform tensile ductility in nanocrystalline metals. Phys. Rev. Lett. 105, 215502.
Wang, Y.M., Voisin, T., McKeown, J.T., Ye, J.C., Calta, N.P., Li, Z., Zeng, Z., Zhang, Y., Chen, W., Roehling, T.T., Ott, R.T., Santala, M.K., Depond, P.J., Matthews, M.J., Hamza, A.V., Zhu, T., 2018b. Additively manufactured hierarchical stainless steels with high strength and ductility. Nat. Mater. 17, 63–70.
Wu, Y., Liu, W.H., Wang, X.L., Ma, D., Stoica, A.D., Nieh, T.G., He, Z.B., Lu, Z.P., 2014. In-situ neutron diffraction study of deformation behavior of a multi–component high-entropy alloy. Appl. Phys. Lett. 104, 051910.